DNA Fragmentation Induced in Human Fibroblasts by ^{56}Fe Ions: Experimental Data and Monte Carlo Simulations

Author(s): A. Campa, D. Alloni, F. Antonelli, F. Ballarini, M. Belli, V. Dini, G. Esposito, A. Facoetti, W. Friedland, Y. Furusawa, M. Liotta, A. Ottolenghi, H. G. Paretzke, G. Simone, E. Sorrentino, and M. A. Tabocchini

Source: Radiation Research, 171(4):438-445.
Published By: Radiation Research Society
DOI: http://dx.doi.org/10.1667/RR1442.1
URL: http://www.bioone.org/doi/full/10.1667/RR1442.1

RADIATION RESEARCH **171**, 438–445 (2009)
0033-7587/09 $15.00

DNA Fragmentation Induced in Human Fibroblasts by ^{56}Fe Ions: Experimental Data and Monte Carlo Simulations

A. Campa,[a,1] D. Alloni,[b,c] F. Antonelli,[a] F. Ballarini,[c] M. Belli,[a] V. Dini,[a] G. Esposito,[a] A. Facoetti,[c] W. Friedland,[d] Y. Furusawa,[e] M. Liotta,[f] A. Ottolenghi,[c] H. G. Paretzke,[d] G. Simone,[a] E. Sorrentino[a] and M. A. Tabocchini[a]

[a] *Health and Technology Department, Istituto Superiore di Sanità, and INFN Sezione di Roma1, Gruppo Collegato Sanità, Roma, Italy;* [b] *Laboratory of Applied Nuclear Energy, Università degli Studi di Pavia, Italy;* [c] *Nuclear and Theoretical Physics Department, Università degli Studi di Pavia, and INFN Sezione di Pavia, Italy;* [d] *Helmholtz Zentrum München, Institute of Radiation Protection, Neuherberg, Germany;* [e] *National Institute for Radiological Sciences, Chiba, Japan; and* [f] *Physics Department, Università degli Studi di Milano, and INFN Sezione di Pavia, Italy*

Campa, A., Alloni, D., Antonelli, F., Ballarini, F., Belli, M., Dini, V., Esposito, G., Facoetti, A., Friedland, W., Furusawa, Y., Liotta, M., Ottolenghi, A., Paretzke, H. G., Simone, G., Sorrentino, E. and Tabocchini, M. A. DNA Fragmentation Induced in Human Fibroblasts by ^{56}Fe Ions: Experimental Data and Monte Carlo Simulations. *Radiat. Res.* 171, 438–445 (2009).

We studied the DNA fragmentation induced in human fibroblasts by iron-ion beams of two different energies: 115 MeV/nucleon and 414 MeV/nucleon. Experimental data were obtained in the fragment size range 1–5700 kbp; Monte Carlo simulations were performed with the PARTRAC code; data analysis was also performed through the Generalized Broken Stick (GBS) model. The comparison between experimental and simulated data for the number of fragments produced in two different size ranges, 1–23 kbp and 23–5700 kbp, gives a satisfactory agreement for both radiation qualities. The Monte Carlo simulations also allow the counting of fragments outside the experimental range: The number of fragments smaller than 1 kbp is large for both beams, although with a strong difference between the two cases. As a consequence, we can compute different RBEs depending on the size range considered for the fragment counting. The PARTRAC evaluation takes into account fragments of all sizes, while the evaluation from the experimental data considers only the fragments in the range of 1–5700 kbp. When the PARTRAC evaluation is restricted to this range, the agreement between experimental and computed RBE values is again good. When fragments smaller than 1 kbp are also considered, the RBE increases considerably, since γ rays produce a small number of such fragments. The analysis performed with the GBS model proved to be quite sensitive to showing, with a phenomenological single parameter, variations in double-strand break (DSB) correlation.

[1] Address for correspondence: Health and Technology Department, Istituto Superiore di Sanità Viale Regina Elena, 299-00161 Roma, Italy; e-mail: campa@iss.infn.it.

INTRODUCTION

In experiments studying the response of cells to irradiation with high-LET charged particles, one can consider end points such as cell death, gene mutations and chromosome aberrations as well as the level of initial DNA damage. It is commonly accepted that late end points are a direct consequence of the initial damage processing, and in particular of DNA double-strand breaks (DSBs) (*1–3*). However, it has been found that the RBE for initially induced damage and the RBE for the late end points cited above are very different, the former being generally between 1 and 2 (*4*), much smaller than the latter, which have been found to reach values up to about 10 (*5–8*). To explain this, the hypothesis has been put forward that not only the number of DSBs but also their distribution along the genome strongly affects the cell fate; in particular, the reparability of a DSB could be affected by the nearness, both spatial and genomic, of other DSBs (*3*). Their distribution after irradiation with a densely ionizing radiation is expected to be different from that resulting by a random insertion of DSBs, since the DSBs caused by a given track will be spatially correlated. The correlation will also be determined by the chromatin conformation, and since this conformation is quite complex, forming several structures at different size scales, from the nucleosome to the chromatin fiber loops, the statistical properties of the DSB distribution are not simple. Indeed, while for low-LET radiation we expect to find DSB correlation at the nucleosome size scale (*9–11*) and perhaps up to a few kbp (*12*), the DSB distributions after exposure to high-LET radiation can also deviate from randomness at large (more than 10 kbp) size scales (*13–17*). It must be emphasized that, even if these statistical properties could be determined exactly, one would still face the problem of establishing which of them have more influence on the processes related to the repair of damage and therefore on the cellular end points; in other words, one should find evidence regarding which correlation size scale has more in-

fluence on decreasing the efficiency of the repair machinery.

In spite of this constraint, it is clear that a refined determination of the DSB distribution is an important step in the study of the cellular response to high-LET radiation, an issue that is very important in the framework of radiation protection (particularly in space, in the case of long-term manned missions) and of radiation therapy. In this context, we studied the DNA fragmentation spectra produced in human fibroblasts by two different iron-ion beams, one of energy 414 MeV/nucleon, and the other of energy 115 MeV/nucleon (with dose-averaged LETs in water equal to 202 keV/μm and 442 keV/μm, respectively). The study was performed by analyzing the experimental spectra and by comparing them with those computed using the Monte Carlo PARTRAC simulation code (*18*), which was recently upgraded to simulate ions heavier than α particles (*19*). Using this code, we also determined the spectra outside the experimentally observable DNA fragment size range (we note that the fragment spectra are a direct consequence of the DSB distribution). The purpose of the first part of our work, i.e., of the comparison between experimental and computed fragmentation spectra, is mainly the pursuit of a validation of the recent extension of the PARTRAC code to heavy ions; the motivation of the second part, i.e., of the evaluation of the spectra outside the experimental range, is the determination, as complete as possible, of the statistical properties of the distribution of the DNA damage. Obviously, to be sufficiently confident in the data produced by the code outside the experimental part, the comparison in the observable range must give a satisfactory agreement. We will show that this is the case. The experimental data concern several doses up to 200 Gy, and the range of fragment sizes is 1–5700 kbp. The analysis of the simulation data outside this range is important basically for the fragments smaller than 1 kbp, since for the doses under examination the number of fragments larger than 5700 kbp is negligible. It will be shown that, including the fragments smaller than 1 kbp, the RBE for DSB production increases considerably, especially for the beam with the highest LET. To compute these RBE values, we used the experimental data (in the same size range 1–5700 kbp) and the PARTRAC data for the fragment spectra after γ irradiation. The marked increase of the RBE for DSB production when the very small fragments (<1 kbp) are included in the evaluation makes its value closer to the RBE values observed for the late cellular effects cited previously, although the difference is still pronounced, probably due to DSBs at distances below a few tens of bp, often described as ''complex lesions'' (*20*), or DSB++ (*21*). As we argue in the Discussion, this fact must be taken into consideration when trying to make a correlation between the level of a given late cellular effect and the number of such complex lesions.

In addition to the comparison with the Monte Carlo simulations, our analysis of the experimental data includes the computation of phenomenological parameters that are related to the spatial correlation of the radiation-induced DSBs. This calculation is based on the generalized broken stick (GBS) model (*22*). The information provided in this way is then put in correspondence with that obtained with the simulations.

The agreement between the experimental data and the PARTRAC simulation data was satisfactory for both iron-ion beams, in particular if we consider that no adjustable parameter is fitted *a posteriori* in the Monte Carlo code, after they have been fixed for photon irradiation. Outside the experimentally observable range, the most interesting result is the large value and large LET variation of the number of fragments smaller than 1 kbp.

MATERIALS AND METHODS

Cell Culture

AG1522 diploid primary human fibroblasts (Coriell Institute for Medical Research) were grown as monolayers in α-MEM supplemented with 1 m*M* glutamine, 20% fetal calf serum, 2% Hepes buffer solution (1 *M*), and 50 U/dm^3 of penicillin and streptomycin. Cells used for detection of fragments in the size range 23–5700 kbp were cultured for at least five generations in the presence of 1.85×10^3 Bq/cm^3 [^{14}C]thymidine (Nunc) to reach and maintain confluence. Cells used for detection of fragments in the size range 1–23 kbp were seeded at higher density and cultured for three generations in the presence of 1.85×10^4 Bq/cm^3 [^{3}H]thymidine. The labeled medium was replaced with unlabeled medium 24 h before irradiation. Cells were then detached and suspended at a final concentration of about 1.3×10^6 cells/cm^3 in 0.8% (w/v) low-gelling agarose (Sigma Type VII, Sigma Aldrich) made up in PBSS/EDTA buffer. A volume of 85 μl of this suspension was pipetted into $7 \times 5 \times 2$-mm moulds (Bio-Rad) and allowed to form plugs at 4°C.

Irradiation

Cells embedded in agarose plugs were irradiated at 4°C with one of the two iron-ion beams at the Heavy Ion Medical Accelerator (HIMAC) of the National Institute of Radiological Sciences (NIRS), Chiba, Japan. The maintenance of samples at low temperature to prevent DNA DSB repair during irradiation was accomplished by the use of plug holders that were especially designed to fit the slot of the T-25 flask holder at HIMAC. Such plug holders have a pocket on the back where ice is put to refrigerate the plugs. The iron-ion energies at the cell entrance were 414 MeV/nucleon and 115 MeV/nucleon, corresponding to dose-averaged LETs in water of 202 keV/μm and 442 keV/μm, respectively; doses up to 200 Gy were delivered at a dose rate of about 10 Gy min^{-1}; ^{60}Co γ rays were used as the reference radiation at the Istituto Superiore di Sanità (Roma, Italy); in this case, cells were embedded in agarose plugs and irradiated at 4°C, and the dose rate was about 3.5 Gy min^{-1}.

DNA Fragmentation Spectra

DNA fragmentation spectra were measured by gel electrophoresis using four different electrophoresis conditions, each optimized for the detection of fragments in a particular size range. Three different conditions of calibrated pulsed-field gel electrophoresis (PFGE) were used to detect DNA fragments in the size ranges 9–23 kbp, 23–1000 kbp, and 1000–5700 kbp, respectively; constant-field gel electrophoresis (CFGE) was used for the detection of the smallest fragments (size range 1–9 kbp).

After irradiation, both ^{14}C- and ^{3}H-labeled cells embedded in agarose plugs were incubated in lysis solution (0.5 mol dm^{-3} EDTA, pH 8.0, 1% sarkosyl, 0.5–1.0 mg ml^{-1} proteinase K) for 1 h at 4°C followed by overnight incubation at 50°C. After lysis, the plugs were washed with TE

buffer and then stored in 0.5 mol dm^{-3} EDTA solutions, pH 8.0, with the exception of the plugs used to detect 1–9-kbp fragments, which were not washed but were instead kept in lysis solution to avoid the loss of very small fragments.

DNA damage was evaluated by calibrated PFGE or CFGE using a CHEF DRIII system (Bio-Rad). To separate large DNA fragments (1000–5700 kbp), PFGE was performed in 0.75× TAE buffer (40 m*M* Tris-acetate, 2.0 m*M* EDTA, pH 8.0) at 14°C for 44 h at 2 V/cm (switch time 1200 to 2400 s, angle 106°) followed by 4 h at 6 V cm^{-1} (switch time 7 to 114 s, angle 120°). To separate intermediate and small DNA fragments (23–1000 kbp, 9–23 kbp), PFGE was performed in 0.5× TBE buffer (44.5 m*M* Tris, 44.5 m*M* boric acid, 1.0 m*M* EDTA, pH 8.0). In the former case the run was carried out at 14°C for 18 h, 6 V cm^{-1} (switch time 50 to 90 s, angle 120°) and in the latter case at 14°C for 13 h, 7 V cm^{-1} (switch time 0.5-0.9 s, angle 120°). CFGE was used to separate very small fragments (1–9 kbp). Plugs and their lysis solutions were loaded in separate wells on the same 1% agarose gel in 1× TAE buffer at 3.5 V cm^{-1} for 2 h at room temperature.

For both PFGE and CFGE, suitable size markers were used for gel calibration, Low Range PFG Marker (BioLabs) and 1 kbp DNA Ladder Marker (Gibco, Invitrogen) for PFGE, 100 bp DNA Ladder Marker (Gibco, Invitrogen) and DNA Size Standard 8–48 kb (Bio-Rad) for CFGE.

After electrophoresis, each gel lane was cut in accordance with the specific molecular weight markers chosen to have conveniently spaced zones; in turn, each zone was divided in several slices. Each slice was incubated in scintillation vials with 0.5 cm^3 of 1 *M* HCl and kept overnight at 70°C to allow the gel to melt. Then 7 ml scintillation cocktail (Ultima Gold XR) was added to each sample, and the ^{14}C or ^{3}H activity was measured using a liquid scintillation β-particle counter.

The fraction of DNA mass in each slice was derived by the normalized activity in that slice, and the corresponding number of fragments was evaluated by dividing the fraction of DNA mass by the mean molecular weight of that slice. Then the total number of fragments (almost equal to the total number of DSBs) induced in each size range was obtained by summing up the contributions of the different slices considering both electrophoresis conditions. More details on the experimental procedure and DSB calculation can be found in ref. (*17*).

Monte Carlo Simulations and Analysis of Data

The experimental data were analyzed in two ways. The first was through the comparison of the fragment spectra with the results obtained in Monte Carlo simulations with the PARTRAC code (*18*); the second was by the derivation, from the experimental spectra, of parameters related to the DSB correlation employing the GBS model (*22*). Both theoretical approaches have been described elsewhere; we summarize here a few relevant details and refer the interested reader to refs. (*18*) and (*22*) for more information.

The biophysical simulation code PARTRAC combines an event-by-event description of the radiation track structure in liquid water at the nanometer level with an atom-by-atom representation of the biological target (*18*). The current version (*19*) simulates the transport and interactions of photons, electrons, protons, helium ions and heavier ions. In the simulations, the DNA target represents the whole genome (about 6 Gbp) of a diploid human fibroblast in its interphase, using six levels of DNA organization (deoxynucleotide pair, double helix, nucleosome, chromatin fiber, chromatin fiber loops and chromosome territories). This model nucleus, embedded in a water environment, was irradiated with a parallel beam, and the dose was calculated from the sum of the energies released in all deposition events, assuming a nucleus density of 1.06 g/cm^3. The radiation-induced DNA strand breaks were determined by the superposition of the track structure pattern of inelastic events with the DNA target model. A strand break can be produced by a direct (and ''quasi-direct'') effect or by an indirect effect. It was assumed that a single-strand break (SSB) may be produced by an inelastic energy deposition larger than 5 eV in the volume occupied by the sugar-phosphate backbone (direct effect) or in the water shell surrounding the double helix (quasi-direct effect); the probability of producing an SSB is 1 if the released energy is larger than 40 eV, and it increases linearly from 0 to 1 for energies between 5 eV and 40 eV. An SSB is produced by an indirect effect, with a probability of 65%, by the interaction with the sugar-phosphate backbone of an $^{\bullet}OH$ resulting from ionized or excited water molecules. A DSB was assumed to occur when two SSBs were found on opposite strands within 10 bp. At the end of each simulation, the length of fragments was determined from the genomic distances between two adjacent DSBs (that could have been produced by the same ion track or by two different ion tracks) or between a DSB and a chromosome end; the number of fragments for each size range was then obtained.

The starting consideration in the GBS model was as follows: Not all the DSBs revealed through electrophoresis are induced by the radiation. In the genome, there are always endogenous breaks. Other breaks are caused by the procedures related to the electrophoresis itself. This is modeled by randomly inserting the radiation-induced DSBs on an ensemble of DNA molecules whose size distribution is equal to the fragment size distribution measured in the control sample (suitable extended to sizes above the experimental size range). The plausible motivations and the limitations of this method have been discussed elsewhere (*22*). A similar treatment for the background fragmentation is found in ref. (*23*); a procedure for systematic subtraction of the background DSBs is given in ref. (*24*). The relevant point here is how the model is used to extract parameters related to the DSB correlation from the experimental data. In a random insertion of the DSBs, the governing quantity is the yield, i.e., the number of radiation-induced DSBs per unit dose and unit DNA length. The following three size ranges were chosen: 1–9 kbp for small fragments, 145–750 kbp for intermediate fragments, and 750–2700 kbp for large fragments. These ranges were chosen because we wanted to have three ranges associated, respectively, with small, intermediate and large fragments without the need to cover the full experimental range; the somewhat larger experimental uncertainties in the size range 9–23 kbp and for sizes larger than 2700 kbp suggested our choice. The number of fragments in each of the three ranges and for each experimental dose was computed with the GBS model, leaving the yield as a free parameter. Therefore, for each size range and for each dose, the model gave the corresponding number of fragments as a function of the yield. Optimizing the value of the yield by fitting the computed number of fragments to the measured number (for each size range and for each dose), three dose-dependent yields were computed, denoted by y_1, y_2 and y_3 and corresponding to the three ranges 1–9 kbp, 145–750 kbp and 750–2700 kbp, respectively. These yields, as shown below, are the basis of the data analysis.

RESULTS

For the two iron-ion beams, we obtained experimental data in the range 40–200 Gy for the two size ranges 23–1000 kbp and 1000–5700 kbp, while for the two size ranges 1–9 kbp and 9–23 kbp, the data were obtained in the range 100–200 Gy. By plotting the number of fragments in the size ranges 1–23 kbp and 23–5700 kbp as a function of dose, the data can be fitted very well with a linear function, so that it is possible to define separate radiation-induced DNA DSB yields in these two ranges; the yields are given by the slopes of the fitting lines. These measured values for the DNA DSB yields are reported in the first and third rows of data in Table 1 (for the 115 and 414 MeV/nucleon beams, respectively). The plots themselves are shown in Fig. 2 below and will be discussed later, together with the PARTRAC simulations. The column ''all sizes'' in Table 1, which for the experimental data concerns fragments in the range 1–5700 kbp, gives the total experimental yield,

TABLE 1
DNA DSB Yields, in Units of (Gy Gbp)$^{-1}$, Evaluated in Various Size Ranges, Obtained from Experimental Data and from Simulation Data

Radiation type	<1 kbp	1–23 kbp	23–5700 kbp	>5700 kbp	All sizes	RBE
Iron ions, 115 MeV/nucleon Experimental		2.50 ± 0.74	5.76 ± 0.41		8.26 ± 0.85 (1–5700 kbp)	1.34 ± 0.17 (1–5700 kbp) 1.09 ± 0.12 (23–5700 kbp)
Iron ions, 115 MeV/nucleon PARTRAC	8.99	2.10	5.29	0.35	16.73	2.39 (All sizes) 1.15 (1–5700 kbp) 0.87 (23–5700 kbp)
Iron ions, 414 MeV/nucleon Experimental		2.27 ± 0.49	7.14 ± 0.58		9.41 ± 0.76 (1–5700 kbp)	1.52 ± 0.16 (1–5700 kbp) 1.36 ± 0.15 (23–5700 kbp)
Iron ions, 414 MeV/nucleon PARTRAC	2.90	2.13	8.26	0.11	13.40	1.91 (All sizes) 1.62 (1–5700 kbp) 1.35 (23–5700 kbp)
Gamma rays Experimental		0.90 ± 0.18	5.27 ± 0.41		6.17 ± 0.45 (1–5700 kbp)	
Gamma rays PARTRAC	0.30	0.31	6.10	0.30	7.01	

Notes. The data on γ rays, only partially plotted in this work in Fig. 3, are from refs. (*4, 22*). The last column gives the RBE values in the different size ranges.

i.e., the sum of the two partial yields. From these values it is possible to evaluate the fraction of small fragments in the range 1–23 kbp with respect to the total number of fragments in the range 1–5700 kbp. It turns out that for the 115 MeV/nucleon iron ions the small fragments (1–23 kbp) represent about 30% of the total, while for 414 MeV/nucleon iron ions they represent about 24% of the total. The fifth row of data in Table 1 shows the corresponding values for γ rays, and one can see that in this case the small fragments decrease to about 15% of the total. Table 1 contains also the RBE values for DSB induction, i.e., the ratio between the DSB yield for iron ions and that for γ rays, and the data obtained from the PARTRAC simulations. We discuss these further data together below.

Analysis of Data

The basic idea in the use of the parameters y_1, y_2 and y_3, introduced previously in the Materials and Methods, was that they should all be equal and independent of dose if radiation produced a random distribution of DSBs. One expects that the more the ratio between DSB yields evaluated in two size ranges is different from 1, the more DSBs are induced nonrandomly by radiation. As a rule of thumb, it is possible to say that if y_i is greater than y_j, then the DSB correlation at the length scale corresponding to the ith size range is larger than at the length scale corresponding to the jth size range. We therefore defined the two ratios $R_s = y_1/y_3$ and $R_m = y_2/y_3$ and studied them as a function of dose for all radiation qualities. The subscripts s and m recall that R_s and R_m give information on ''small'' and ''medium'' fragments, respectively.

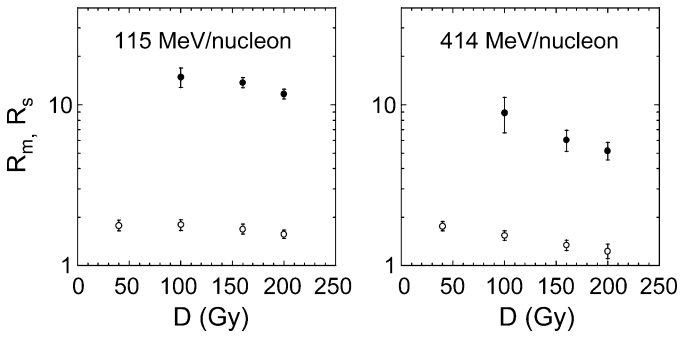

FIG. 1. Parameters R_m (open circles) and R_s (full circles) plotted on a semilog scale as a function of dose. Error bars are obtained by error propagation from experimental data. These parameters are defined by $R_s = y_1/y_3$ and $R_m = y_2/y_3$, where y_1, y_2 and y_3 are the yields of fragments in the size ranges 1–9 kbp, 145–750 kbp and 750–2700 kbp, respectively. These yields are computed by a fitting procedure in the framework of the GBS model, as explained in the text. Error bars are SE.

In Fig. 1, the values of R_m and of R_s are given for 414 and 115 MeV/nucleon iron ions. We first discuss the results for R_m. Taking into account the size of the propagated experimental errors, we can say that for both energies the parameter R_m is significantly larger than 1. For 414 MeV/nucleon iron ions, R_m shows a marked decrease with dose, while the decrease for 115 MeV/nucleon iron ions is much less pronounced. We can therefore conclude the following. The DSBs induced by both iron-ion beams are more correlated in the range 145–750 kbp than in the range 750–2700 kbp; for doses higher than 100 Gy, it appears that this difference in correlation tends to decrease for 414 MeV/nucleon iron ions, while it remains almost the same for 115 MeV/nucleon iron ions (at least for the doses considered in our experiments). The data for γ rays (not plotted) show that, considering the experimental uncertainty on R_m, no difference between the two size ranges can definitely be inferred.

The results for R_s for to the size range 1–9 kbp are very interesting. In this case the difference between the two iron-ion beams is considerable. The R_s values for 115 MeV/nucleon iron ions are between 10 and 15, while those for 414 MeV/nucleon iron ions are between 5 and 10; this points to a DSB correlation at the scale 1–9 kbp that is significantly higher at each dose for 115 MeV/nucleon iron

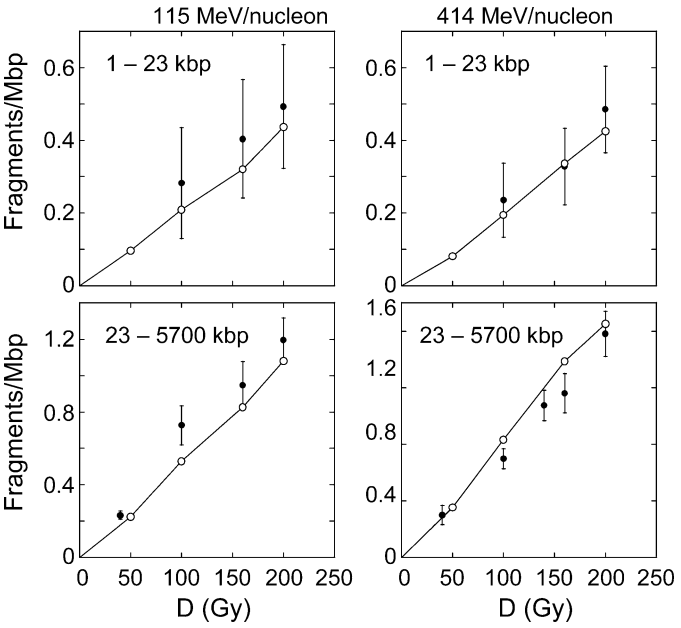

FIG. 2. Number of fragments per Mbp as a function of dose for 115 and 414 MeV/nucleon iron-ion beams in the two size ranges indicated. Full circles: experimental data with error bars. Open circles: PARTRAC data; these data are linked by lines as a guide to the eye. Error bars are SE.

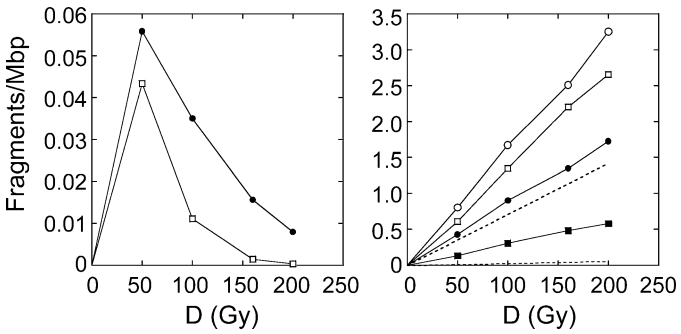

FIG. 3. Left panel: PARTRAC data for the number of fragments per Mbp larger than 5700 kbp for 115 MeV/nucleon iron ions (full circles) and 414 MeV/nucleon iron ions (open squares). Right panel: PARTRAC data for the number of fragments per Mbp of size less than 1 kbp and of all sizes. Open circles and open squares: total numbers of fragments of all sizes for 115 and 414 MeV/nucleon iron ions, respectively. Full circles and full squares: numbers of fragments smaller than 1 kbp for 115 and 414 MeV/nucleon iron ions, respectively (lines are a guide to the eye). The upper and lower dashed lines represent the total numbers of fragments of all sizes and numbers of fragments smaller than 1 kbp for γ rays, respectively.

ions than for 414 MeV/nucleon iron ions. Comparing the R_s values and R_m values for each dose, we see that the former are much larger than the latter, indicating that iron ions induce DSBs more strongly correlated at the scale 1–9 kbp than at the scale 145–750 kbp. The data for γ rays (not plotted), indicate some DSB correlation at the scale 1–9 kbp only for the highest dose; such an effect, due to the proximity of two DSBs in a short piece of a chromatin fiber, has been calculated in ref. (*12*).

We expect that both R_m and R_s will decrease to 1 (i.e., toward the value characterizing a random insertion of DSBs) at sufficiently high doses for both radiation qualities, when many independent tracks contribute to DSB production; besides, it is not surprising that this decreasing trend, in the dose range studied here, is more evident for the radiation with lower LET. However, we cannot produce a quantitative argument to predict the dose range where, for a given radiation quality, the two parameters will be practically equal to 1.

PARTRAC Simulations

Plots of the number of fragments (normalized per Mbp) as a function of dose, as obtained from the experimental data and as computed in the PARTRAC simulations, are shown in Fig. 2. In this and the following figures, no error bars are shown for the Monte Carlo data, since the computed statistical errors are contained within the symbol size. The calculated data are within the experimental uncertainty for the size range 1–23 kbp for both energies; for the size range 23–5700 kbp we note that PARTRAC data underestimate experimental data for 115 MeV/nucleon iron ions slightly, while there is a small overestimation for 414 MeV/nucleon iron ions. However, emphasizing again that no *a posteriori* adjustment in the code parameters was done, after their fixing in the case of photon irradiation, we conclude that the agreement can be considered satisfactory for both energies.

As pointed out earlier, this good result led us to study the PARTRAC data outside the experimental size range. The number of fragments larger than 5700 kbp is plotted in the left panel of Fig. 3; we see that this number (small for all our doses) decreases with increasing dose. This decrease of the larger fragments with dose is to be expected, since the increasing number of DSBs with dose will decrease the probability that a large DNA fragment will remain free of DSBs. In the right panel of the figure, we show the number of fragments smaller than 1 kbp and the total number of fragments. Three things should be emphasized for fragments smaller than 1 kbp. The first is their large number for both iron-ion energies; the second is that, within this large contribution in both cases, the relative weight with respect to the total number of fragments is very different: about 50% for 115 MeV/nucleon iron ions and somewhat more than 20% for 414 MeV/nucleon iron ions. We argue that this large difference reflects the difference in the track structure. In fact, the more energetic (on average) secondary electrons created by the more energetic beam should travel further (on average) from the track core, and this could decrease, with respect to the less energetic beam, the number of very small fragments. Finally, the total number of fragments caused by γ rays is roughly half of that caused by iron ions at the corresponding dose, and the number of fragments smaller than 1 kbp is small, as seen in Fig. 3.

The PARTRAC results and their comparison with the

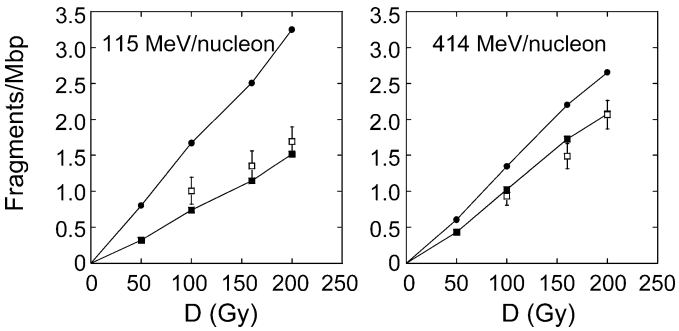

FIG. 4. Number of fragments per Mbp for experimental data with error bars in the whole observable range 1–5700 kbp (open squares) and PARTRAC data in the range 1–5700 kbp (full squares); PARTRAC data in the entire range (full circles). PARTRAC data are linked by lines as a guide to the eye. Error bars are SE.

experimental data are summarized in Table 1. In contrast with what was done in the case of the experimental data, we computed the PARTRAC yields in the different ranges by simply dividing the results for the number of fragments per Mbp obtained for 100 Gy by 100; this does not introduce appreciable effects on the comparison with the experimental yields, since, as for the latter data, the PARTRAC results in the ranges 1–23 kbp and 23–5700 kbp are very well represented by a linear function. This also happens, as seen in the right panel of Fig. 3, for the PARTRAC data for fragments smaller than 1 kbp; the corresponding yields are given in the first column of data in Table 1. Obviously this is not true for fragments larger than 5700 kbp (left panel of Fig. 3), and, as a consequence, the yield defined as above is not reliable (or better, no yield should be defined) for this size range. However, the very small number of such large fragments makes this incorrect definition quantitatively irrelevant for our purposes. It should be clear that experimental RBEs shown in Table 1 were obtained using the experimental yields for both the iron-ion beams and γ rays, while the PARTRAC RBEs were obtained using PARTRAC yields for both the iron-ion beams and γ rays. The following should be noted. For both iron-ion beams, the PARTRAC values are within the corresponding experimental values when error bars are considered (apart from a deviation for 23–5700 kbp for 115 MeV/nucleon iron ions). However, taking into account all sizes in the simulations (which essentially means taking into account fragments smaller than 1 kbp), the RBE increases considerably; in fact, not counting fragments smaller than 1 kbp strongly underestimates the yield, since the number of such small fragments is small in the case of γ rays. Consistent with the difference in the yield of these small fragments for the two iron-ion beams, the difference between the PARTRAC yield for all sizes and the experimental yield is larger for 115 MeV/nucleon iron ions.

To complete the comparison, in Fig. 4, we show the total experimental numbers of fragments and the PARTRAC values in the experimental range 1–5700 kbp and for fragments of all sizes. We note that the slight PARTRAC underestimation and overestimation in the size range 23–5700 kbp for 115 and 414 MeV/nucleon iron ions, respectively, is decreased when we consider the total experimental range 1–5700 kbp.

DISCUSSION

This work is a part of our research program in which we plan to study the DNA fragment spectra produced by different radiation qualities, with an integrated approach that includes the analysis of the experimental spectra with the GBS model and their comparison with the PARTRAC-simulated spectra. We have already considered low-energy proton and α-particle beams (*25*), and we have recently begun to study iron ions (*26*), taking advantage of the extension of the PARTRAC code (*19*).

As we explained in the Introduction, our purpose is twofold: to validate the simulation code and to characterize the spectra, both with the phenomenological description of the GBS model and with the computation of the numbers of small fragments smaller than 1 kbp.

In addition to the validation obtained for light ions, this further validation for heavy ions like iron is important, since the PARTRAC code, even if it is considered to be an *ab initio* Monte Carlo code, without *a posteriori* parameter adjustments (after the original values for photon radiation), relies on quantities that have not yet been firmly established, such as the probability of formation of an SSB by a direct energy deposition or by an $^{\cdot}$OH attack or the genomic distance of two SSBs on opposite strands forming a DSB. On the other hand, the experimental data also suffer from the presence of uncertainty sources. The most relevant are the presence of a background fragmentation and the probable induction of extra DSBs during the measurement procedures (*27*). The first factor prevents the comparison of detailed experimental spectra (i.e., with narrow size ranges) with PARTRAC simulations, where radiation interacts with an intact genome. However, in larger size ranges such as those presented in Fig. 2 (with the extension of a size range measured relative to its average size) the radiation-induced DSBs can be computed experimentally by subtraction, and the comparison with the simulations can be performed. The second factor, e.g., the presence of heat-labile sites, while it could lead to an overestimation of the DSB yield in the measured size range (*27, 28*), should affect the RBE values, given by a ratio of yields, much less (although it is not clear whether heat-labile sites are produced at different rates by γ rays and heavy ions).

The phenomenological analysis provided by the GBS model takes into account the background fragmentation when extracting the parameters characterizing nonrandom DSB induction from the experimental data, which indicate the length scales at which DSBs are more correlated. In this sense, this approach can be considered to be complementary to the PARTRAC simulations. It is useful to make a comparison with a recent study (*29*) in which DNA frag-

mentation spectra after irradiation with nitrogen-ion beams of several different of LETs were analyzed using the RLC model (*30*). This model assumes that the DSB pattern is the result of the distribution of DSB clusters along the genome; while the clusters are randomly located, the distribution of fragment lengths caused by the DSBs in a cluster follows a certain probability function. The difference between radiation qualities should be described by the differences in the features of this probability function and in the mean number of DSBs per cluster. Although the radiation qualities studied in ref. (*29*) are different from those considered here, some relevant results are similar; in particular, the nonrandom nature of DSB induction by the nitrogen ions is represented by the fitted mean number of DSBs per cluster (*29*), which is definitely larger than 1 (1 DSB per cluster is equivalent to the broken stick model, i.e., to randomly located DSBs). Also, a decrease with dose in the number of large fragments is also seen; in the RLC model, this is explained mechanistically by the interlacing of clusters.

The statistical properties of the radiation-induced DSBs, and thus the fragment spectra, do not depend only on LET. In fact, for a given spatial organization of the target DNA, the DSB spectrum will depend on the track structure, which in turn is not uniquely determined by the LET of the radiation (*19*). In particular, radiations with similar (high) LET can have very different track structures, if, e.g., they are made of ions of quite different charges. This indicates that each radiation quality should in principle be studied separately. More practically, one should consider as many different cases as possible. As mentioned above, we have begun this effort with the study of low-energy light ions, and we have recently turned our attention to higher-energy heavier ions.

The two high-LET iron-ion beams considered in this work show interesting differences that can be observed in Table 1 and Fig. 1. The intricate relationship between the target pattern and track structure, mentioned above, does not allow us to make reliable predictions based on the DSB yield in a partial size range of the DSB yield in another partial size range. We have a manifestation of this in the PARTRAC data for the two lower size ranges. We see in Table 1 that, while the yield of fragments in the size range 1–23 kbp is similar for the two iron-ion beams, as also found experimentally, the yield of fragments smaller than 1 kbp is considerably larger for the higher-LET beam, being about half of the total yield. One can argue that the higher energy of the lower-LET beam causes a larger radius of the tracks, and this in turn causes a smaller interaction with the lowest levels of the DNA spatial organization. However, when we look at the DSB correlation using the parameter R_s of the GBS model instead of at the DSB yield, we also find a large difference between 115 MeV/nucleon iron ions and 414 MeV/nucleon iron ions in the experimental size range 1–9 kbp. This is a further confirmation that the information provided by the two computational approaches is complementary; in particular, the GBS model appears to be quite sensitive to variations in DSB correlation.

The PARTRAC simulation data show that, both for 115 and 414 MeV/nucleon iron ions, the RBE for DSB induction is greatly underestimated in the experimental determination, which does not count fragments smaller than 1 kbp. The higher PARTRAC values are still far from the RBE values for the late cellular end points referred to at the beginning, i.e., aberrations, mutations and cell death. The strong dependence on radiation quality of these late effects, much higher than that of DSB induction, could be explained by the damage processing after irradiation and by the dependence of this processing on the initial damage pattern, taking into account the dependence of the yield of complex DNA lesions on radiation quality. In particular, the repair efficiency of a DSB, as mentioned in the Introduction, may depend on the proximity of other DSBs. Therefore, the results of the PARTRAC simulations presented here could be interpreted as follows. The considerably higher RBEs for DSB induction when fragments smaller than 1 kbp are counted should probably be taken into account among the possible reasons for the higher biological effectiveness (for cellular end points) of high-LET radiations. However, at the same time, the still large difference with respect to the RBEs of these late effects is a probable indication that repair of DSBs is hindered when they are in proximity.

ACKNOWLEDGMENTS

This work was partially supported by the European Commission (EC Contract FI6R-CT-2003-RISC-RAD), by the Italian Space Agency (ASI Contract No. 1/014/06/0-MoMa) and by the Istituto Nazionale di Fisica Nucleare (INFN project ‘‘EPICA’’).

Received: April 23, 2008; accepted: November 4, 2008

REFERENCES

1. D. Frankenberg, M. Frankenberg-Schwager, D. Blöcher and R. Harbich, Evidence for DNA double-strand breaks as critical lesions in yeast cells irradiated with sparsely or densely ionizing radiation under oxic or anoxic conditions. *Radiat. Res.* **88**, 524–532 (1981).
2. G. Obe, C. Johannes and D. Schulte-Frohlinde, DNA double-strand breaks induced by sparsely ionizing radiation and endonucleases as critical lesions for cell death, chromosomal aberrations, mutation and oncogenic transformation. *Mutagenesis* **7**, 3–12 (1992).
3. D. T. Goodhead, Initial events in the cellular effects of ionising radiations: clustered damage in DNA. *Int. J. Radiat. Biol.* **65**, 7–17 (1994).
4. M. Belli, A. Campa, V. Dini, G. Esposito, Y. Furusawa, G. Simone, E. Sorrentino and M. A. Tabocchini, DNA fragmentation induced in human fibroblasts by accelerated ^{56}Fe ions of differing energies. *Radiat. Res.* **165**, 713–720 (2006).
5. K. George, M. Durante, H. Wu, V. Willingham and F. A. Cucinotta, *In vivo* and *in vitro* measurements of complex-type chromosomal exchanges induced by heavy ions. *Adv. Space Res.* **31**, 1525–1535 (2003).
6. M. Durante, K. George, G. Gialanella, G. Grossi, C. La Tessa, L. Manti, J. Miller, M. Pugliese, P. Scampoli and F. A. Cucinotta, Cytogenetic effects of high-energy iron ions: dependence on shielding thickness and material. *Radiat. Res.* **164**, 571–576 (2005).

7. R. Lee, E. Nasonova and S. Ritter, Chromosome aberrations yields and apoptosis in human lymphocytes irradiated with Fe-ions of differing LET. *Adv. Space Res.* **35**, 268–275 (2005).
8. D. Bettega, P. Calzolari, L. Doneda, M. Durante and L. Tallone, Early and delayed reproductive death in human cells exposed to high energy iron ion beams. *Adv. Space Res.* **35**, 280–285 (2005).
9. W. R. Holley and A. Chatterjee, Clusters of DNA damage induced by ionizing radiation: formation of short DNA fragments. I. Theoretical modeling. *Radiat. Res.* **145**, 188–199 (1996).
10. W. Friedland, P. Jacob, H. G. Paretzke and T. Stork, Monte Carlo simulation of the production of short DNA fragments by low-linear energy transfer radiation using higher-order DNA models. *Radiat. Res.* **150**, 170–182 (1998).
11. B. Rydberg, W. R. Holley, I. S. Mian and A. Chatterjee, Chromatin conformation in living cells: support for a zig-zag model of the 30 nm chromatin fiber. *J. Mol. Biol.* **284**, 71–84 (1998).
12. W. Friedland, P. Jacob, H. G. Paretzke, M. Merzagora and A. Ottolenghi, Simulation of DNA fragment distributions after irradiation with photons. *Radiat. Environ. Biophys.* **38**, 39–47 (1999).
13. E. Höglund, E. Blomquist, J. Carlsson and B. Stenerlöw, DNA damage induced by radiation of different linear energy transfer: initial fragmentation. *Int. J. Radiat. Biol.* **76**, 539–547 (2000).
14. M. Löbrich, P. K. Cooper and B. Rydberg, Non-random distribution of DNA double-strand breaks induced by particle irradiation. *Int. J. Radiat. Biol.* **70**, 493–503 (1996).
15. H. C. Newmann, K. M. Prise, M. Folkard and B. D. Michael, DNA double-strand break distributions in X-ray and α-particle irradiated V79 cells: evidence for non-random breakage. *Int. J. Radiat. Biol.* **71**, 347–363 (1997).
16. A. L. Ponomarev and F. A. Cucinotta, Chromatin loops are responsible for higher counts of small DNA fragments induced by high-LET radiation, while chromosomal domains do not affect the fragment sizes. *Int. J. Radiat. Biol.* **82**, 293–305 (2006).
17. M. Belli, R. Cherubini, M. Dalla Vecchia, V. Dini, G. Esposito, G. Moschini, O. Sapora, G. Simone and M. A. Tabocchini, DNA fragmentation in V79 cells with light ions as measured by PFGE. I. Experimental results. *Int. J. Radiat. Biol.* **78**, 475–482 (2002).
18. W. Friedland, P. Jacob, F. Bernhardt, H. G. Paretzke and M. Dingfelder, Simulation of DNA damage after proton irradiation. *Radiat. Res.* **159**, 401–410 (2003).
19. W. Friedland, P. Jacob, H. G. Paretzke, A. Ottolenghi, F. Ballarini and M. Liotta, Simulation of light ion induced DNA damage patterns. *Radiat. Prot. Dosimetry* **122**, 116–120 (2006).
20. A. Ottolenghi, M. Merzagora and H. G. Paretzke, DNA complex lesions induced by protons and a-particles: track structure characteristics determining linear energy transfer and particle type dependence. *Radiat. Environ. Biophys.* **36**, 97–103 (1997).
21. H. Nikjoo, P. O'Neill, W. E. Wilson and D. T. Goodhead, Computational approach for determining the spectrum of DNA damage induced by ionizing radiation. *Radiat. Res.* **156**, 577–583 (2001).
22. A. Campa, G. Esposito, M. Belli, G. Simone and M. A. Tabocchini, DNA fragmentation in V79 cells irradiated with light ions as measured by pulsed-field gel electrophoresis. II. Simulation with a generalized broken stick model. *Int. J. Radiat. Biol.* **80**, 229–238 (2004).
23. M. Pinto, K. M. Prise and B. D. Michael, A Monte Carlo model of DNA double-strand break clustering and rejoining kinetics for the analysis of pulsed-field gel electrophoresis data. *Radiat. Res.* **162**, 453–463 (2004).
24. A. L. Ponomarev, M. Belli, P. J. Hahnfeldt, L. Hlatky, R. K. Sachs and F. A. Cucinotta, A robust procedure for removing background damage in assays of radiation-induced DNA fragment distributions. *Radiat. Res.* **166**, 908–916 (2006).
25. A. Campa, F. Ballarini, M. Belli, R. Cherubini, V. Dini, G. Esposito, W. Friedland, S. Gerardi, S. Molinelli and M. A. Tabocchini, DNA DSB induced in human cells by charged particles and gamma rays: Experimental results and theoretical approaches. *Int. J. Radiat. Biol.* **81**, 841–854 (2005).
26. D. Alloni, F. Ballarini, M. Belli, A. Campa, G. Esposito, W. Friedland, M. Liotta, A. Ottolenghi and H. G. Paretzke, Modeling of DNA fragmentation induced in human fibroblasts by ^{56}Fe ions. *Adv. Space Res.* **40**, 1401–1407 (2007).
27. B. Rydberg, Radiation-induced heat-labile sites that convert into DNA double-strand breaks. *Radiat. Res.* **153**, 805–812 (2000).
28. B. Stenerlöw, K. H. Karlsson, B. Cooper and B. Rydberg, Measurement of prompt DNA double-strand breaks in mammalian cells without including heat-labile sites: results for cells deficient in nonhomologous end joining. *Radiat. Res.* **159**, 502–510 (2003).
29. H. Fakir, R. K. Sachs, B. Stenerlöw and W. Hofmann, Clusters of DNA double-strand breaks induced by different doses of nitrogen ions for various LETs: Experimental measurements and theoretical analyses. *Radiat. Res.* **166**, 917–927 (2006).
30. R. K. Sachs, A. L. Ponomarev, P. Hahnfeldt and R. L. Hlatky, Locations of radiations-produced DNA double strand breaks along chromosomes: A stochastic cluster process formalism. *Math. Biosci.* **159**, 165–187 (1999).